International Journal of Marine Engineering Innovation and Research, Vol. 11(1), Mar. 2026. 139-146
(pISSN: 2541-5972, eISSN: 2548-1479)

Intelligent Optimization of Fast Boat Hull Form for Resistance Reduction Using CFD and Surrogate-Assisted Algorithms

Romadhoni [1*], Budhi Santoso[2], Muhammad Alimul Hafiz[3]

(Received: 29 January 2026 / Revised: 2 February 2026 / Accepted: 11 February 2026 / Available Online: 7 March 2026)

***Abstract*—** High-speed fast boats operating at high Froude numbers experience rapidly increasing resistance due to coupled viscous and wave-making effects. This study proposes a surrogate-assisted hull-form optimization framework that combines Reynolds-averaged Navier-Stokes (RANS) CFD (SST k-ω) with Gaussian Process Regression (Kriging) to minimize the total resistance of a fast monohull while maintaining displacement and geometric feasibility. The hull geometry was parameterized using four variables: deadrise angle, prismatic coefficient, longitudinal centre of buoyancy (LCB), and bow entrance angle. A set of candidate designs was evaluated by CFD, a surrogate model was trained and validated (R^2 = 0.985, prediction error < 2%), and global optimization was carried out using Genetic Algorithm (GA) and Particle Swarm Optimization (PSO). CFD verification of the best design shows a consistent resistance reduction across Fn = 0–0.75, with a maximum reduction of 14.4% at Fn = 0.65 compared to the baseline hull. The optimized hull exhibits reduced bow pressure peaks and delayed flow separation at the transom. The surrogate-assisted strategy reduces the number of CFD evaluations and lowers the overall computational effort by about 78% while preserving prediction accuracy. R^2=0.992.

Keywords—: fast boat; hull-form optimization; CFD; Gaussian process regression; surrogate model; genetic algorithm; particle swarm optimization; resistance

**Corresponding Author: romadhoni@polbeng.ac.id.*

I. INTRODUCTION

Hull-form optimization is critical for fast boats because small changes in geometry can cause large variations in total resistance at high Froude numbers, affecting speed, fuel consumption, and operational range. When a craft transitions to the semi-planing/planing regime, wave-making and pressure effects interact strongly with viscous drag, making resistance reduction a key design target for high-speed passenger and patrol boats [1]. In this context, geometric sensitivity becomes a key consideration: minor variations in deadrise angle, the number of chines, and transverse step configurations can significantly alter trim, wetted surface area, and overall drag. In general, resistance tends to increase with larger deadrise at high Froude numbers [2]. The longitudinal placement of steps is also influential; the optimal step position is often located around the mid-aft region, while steps placed too close to the transom may reduce trim but can increase drag and wetted area [3]. With increasing speed, planing craft typically experience higher trim and changing heave/sinkage, leading to strong coupling among pressure distribution, wave patterns, and viscous resistance [4]. Moreover, the displacement–semi-planing–planing transition is commonly characterized by peaks in drag and trim within a critical regime (Fr ≈ 0.8–1.2), which represents a particularly sensitive region for design optimization [5].

Computational Fluid Dynamics (CFD) provides detailed flow information that is difficult to obtain experimentally at early design stages, and it is widely used for hull resistance and trim assessment. However, CFD-driven optimization is computationally expensive because many design candidates must be evaluated, and each simulation can be time-consuming for free-surface turbulent flows [6].

Surrogate-assisted optimization addresses this limitation by learning an analytical approximation of the CFD response surface from a limited set of simulations. Techniques such as Kriging/Gaussian Process Regression, response surfaces, and radial basis functions have been applied to hull-form optimization to accelerate design exploration while maintaining acceptable accuracy. Global optimizers such as Genetic Algorithm (GA) and Particle Swarm Optimization (PSO) are commonly combined with surrogates to search non-linear design spaces effectively. For example, a GP-based response-surface approach applied to the KCS hull demonstrated high-accuracy resistance prediction, with CFD high-fidelity verification confirming the surrogate-predicted optimum while requiring only a few dozen CFD samples, thereby achieving substantial computational saving [7]. Similarly, a GPR-based optimization framework with adaptive sampling (SBO-MSE + LCB) reported approximately 46.7% higher efficiency than conventional surrogate-based design methods for minimizing total resistance in a 130k DWT aquaculture vessel [8].

Romadhoni is with the Department of Naval Architecture, Politeknik Negeri Bengkalis, Bengkalis, 28711, E-mail: romadhoni@polbeng.ac.id.

Budhi Santoso is with Department of Naval Architecture, Politeknik Negeri Bengkalis, Bengkalis, 28711, E-mail: budhisantoso@polbeng.ac.id.

Muhammad Alimul Hafiz, Laboratory of Ship Hydrodynamics, Departement of Naval Architecture, Polytechnic of Bengkalis, Indonesia, 28711, Indonesia. E-mail: mhafiz@polbeng.ac.id

This paper presents a Kriging-based intelligent optimization framework for a fast monohull hull form. The framework integrates RANS CFD, surrogate modelling, and GA/PSO optimization, followed by CFD verification of the selected optimum [9]. The main contributions are: (i) a compact parameterization using four key geometric variables, (ii) a validated surrogate model with prediction error below 2%, and (iii) resistance reduction of up to 14.4% over Fn = 0–0.75 with substantially reduced CFD effort [10]. These findings are consistent with prior studies showing that Kriging-based optimization of stern geometry can deliver viscous-drag reductions of at least 5% using a limited number of training points, while also highlighting the importance of appropriate design-variable selection and DoE size for surrogate reliability [11]. In addition, global optimizers such as PSO, GA, and their multi-objective variants are widely employed to effectively explore highly nonlinear design spaces when coupled with surrogate models, enabling efficient search and robust convergence in practical hull-form optimization problems [12].

II. METHOD

A. Study Design

This study applies a surrogate-assisted single-objective optimization to minimize the total resistance coefficient (CR) of a fast monohull at the target operating condition while satisfying practical design constraints. The optimization keeps the displacement consistent with the baseline hull and enforces feasible geometric bounds for all design variables. The workflow consists of [13]: (1) defining hull parameters and bounds, (2) generating an initial design set, (3) running CFD to obtain resistance, (4) training and validating a Kriging (GPR) surrogate, (5) performing global optimization using GA and PSO on the surrogate, and (6) verifying the optimum by CFD. This approach closely parallels prior surrogate-based optimization (SBO) frameworks built on GPR to minimize the total resistance coefficient of offshore aquaculture vessels under constant-displacement and geometric-constraint conditions, where the predicted optimum is subsequently revalidated using high-resolution CFD to ensure fidelity and robustness [14].

Figure 1 shows the baseline fast-boat hull used in this study. The configuration represents a typical deep-V planing hull, which is designed to generate hydrodynamic lift and maintain directional stability at high speed. Sharp chines/strakes help reduce spray and improve planing efficiency, which makes this hull type suitable for inter-island transport and patrol operations.

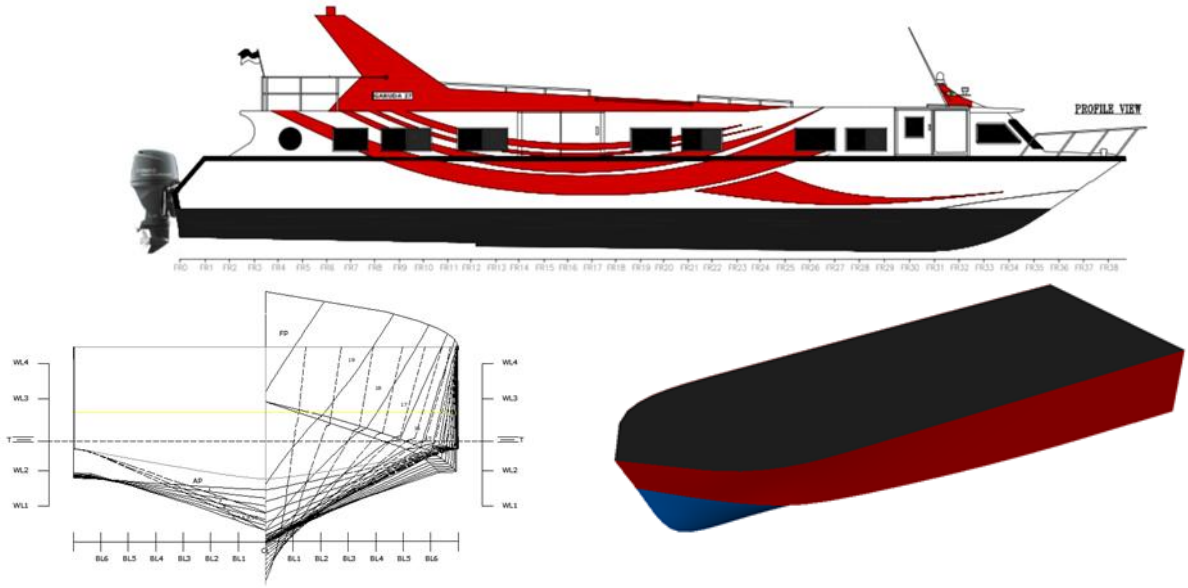

Figure 1. Model Fast Boat

The hull geometry was parameterized using four key variables that strongly influence total resistance in the semi-planing/planing regime: deadrise angle (β), prismatic coefficient (Cp), longitudinal centre of buoyancy position (LCB), and bow entrance angle (α). For hard-chine planing monohulls, increasing β generally increases resistance because it tends to raise wetted surface area and trim, thereby increasing viscous drag and pressure-related contributions [15]. Nevertheless, the effect of deadrise can be configuration-dependent; for certain multihull/pentamaran arrangements, a larger β has been reported to reduce total resistance when the associated reduction in wetted area (and frictional resistance) outweighs the increase in wave-making resistance [16]. The prismatic coefficient Cp is also widely used as a primary descriptor in predictive models of residual and total resistance for planing hulls, often considered alongside key ratios such as L/B and the Froude number [17]. In addition, both CFD and experimental studies consistently identify the longitudinal centre of buoyancy (or LCG/LCB relationship) as one of the most critical parameters

affecting resistance and running attitude [18]. The selected ranges and physical meanings are summarized in Table 1.

TABLE 1.
RESISTANCE COMPARISON

Design Variable	Symbol	Range	Physical Significance
Deadrise angle	β	10° – 25°	Controls planing lift and spray characteristics
Prismatic coefficient	C_p	0.55 – 0.70	Controls longitudinal volume distribution and wave-making
LCB position (from AP, %Lpp)	LCB	45 – 55	Shifts buoyancy distribution and affects trim/resistance
Bow entrance angle	α	15° – 35°	Controls water entry, bow wave, and pressure drag

B. CFD Simulation

CFD simulations were conducted to evaluate resistance for each hull candidate. The solver is based on the incompressible RANS equations with the SST k-ω turbulence model, which is widely used for predicting separation in free-surface flows. Indeed, numerous resistance studies on benchmark hulls such as DTMB 5415, KCS, KVLCC1, REGAL, and Suboff have employed incompressible RANS with the SST k -ω model to predict resistance components, wave patterns, and separation behavior with good agreement against experimental measurements[19]. The SST k−ω model is particularly suitable in this context because of its capability to handle near-wall effects and separation phenomena around the stern and near the free surface under strong pressure-gradient conditions[20]. In terms of numerical implementation, a finite-volume discretization with local mesh refinement around the bow, stern, free surface, and boundary-layer regions is standard practice for ship-resistance simulations and is critical for achieving stable and accurate solutions [21]. Accordingly, the present setup—including the incompressible RANS–SST k−ω formulation, the conventional computational domain and boundary conditions for high-speed craft, and a mesh strategy focused on resolving free-surface and separation features—is consistent with modern marine CFD practice and is supported by extensive validation in the literature.

The numerical domain, boundary conditions, and mesh strategy follow standard practice for high-speed craft resistance simulations, and the setup is illustrated in Figure 2.

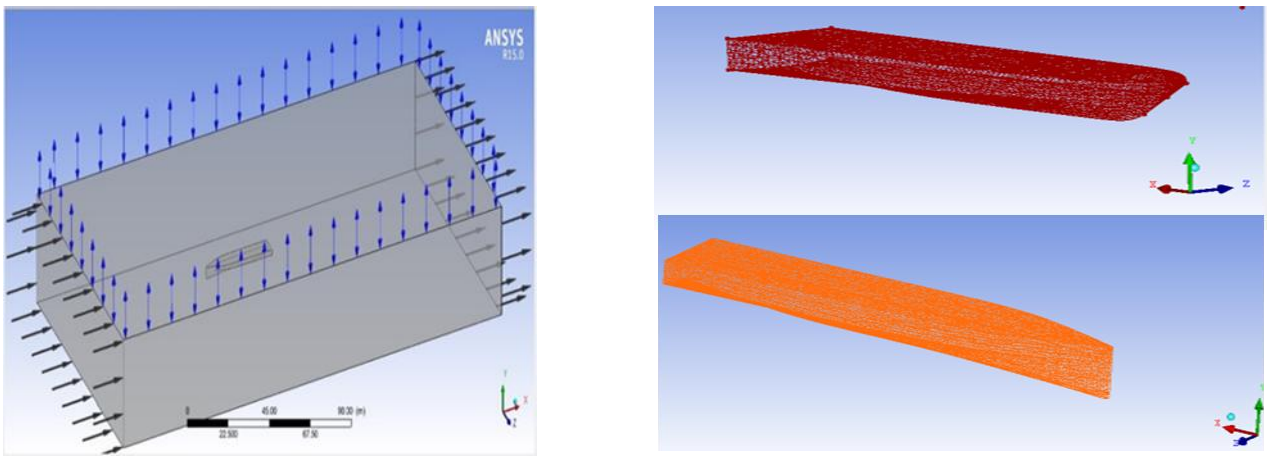

Figure 2. CFD Configuration and Computational Domain

$I_{45}= I_{54} = -\int_M [(x - X_{Cal})] + [(y - Y_{Cal})]dm = M (R_{54}^2 + X_{GC} + Y_{GC})$

The governing equations are: k-ω

$\partial\rho/\partial t+(\partial(\rho u_i))/(\partial x_i)=0$ Continuity: $\nabla\cdot u = 0$ (1)

$(\partial(\rho u_i))/\partial t+(\partial(\rho u_i\ u_j))/(\partial x_j)=-\partial p/(\partial x_i)+\partial/(\partial x_j)$ [μ($(\partial u_i)/(\partial x_j)$ⓜ+$(\partial u_j)/(\partial x_i))$]+ρg_i

Momentum : $\rho(\partial u/\partial t + u\cdot\nabla u) = -\nabla p + \nabla\cdot[(\mu+\mu_t)(\nabla u + (\nabla u)^T)] + \rho g$ (2)

The total resistance is obtained by integrating pressure and shear stress over the wetted surface[22]:R_T

$R_T=\int_S (pn_x+\tau_x)\ dSR_T = \int_S (p\ n_x - \tau_x)\ Ds$ (3)

The total resistance coefficient is computed as: CT

$CT= RT/(1/2\ \rho U^2\ S)$ (4)

$CR = RT / (0.5\ \rho\ U^2\ S\ x\ w)$ (5)

ρ where ρ is fluid density, U is ship velocity, and S_w is wetted surface area.

Simulations were performed using Ansys Fluent 2023R2 with a computational domain size of 6L × 2L × 2L. Boundary conditions include a velocity inlet, pressure outlet, and symmetry planes. Mesh sensitivity analysis indicated convergence at approximately 3.2 million cells. A validation checkfollowing ITTC 2021 procedures resulted in a deviation below 4%. The boundary conditions were specified as a velocity inlet, a pressure outlet, and symmetry planes to reduce computational cost while preserving the dominant flow direction, which is a common practice in external-flow simulations where symmetry can be assumed [23].

C. Surrogate Model Development

To reduce the computational cost of CFD-driven optimization, a surrogate model was built to approximate the relationship between the design variables and the resistance coefficient. After training, the surrogate provides fast resistance predictions and enables extensive exploration of the design space with a limited number of CFD simulations [24]. In the marine hydrodynamics literature, a wide range of surrogate techniques such as artificial neural networks (ANN), Kriging/Gaussian process models, radial basis functions (RBF), and deep neural networks have been trained on CFD-generated datasets to predict total resistance or resistance coefficients from hull-form parameters, including geometry controls based on NURBS or free-form deformation (FFD) representations[25]. After training, the surrogate is typically embedded within an optimization loop (e.g., PSO, NSGA-II, whale or dung-beetle optimizers, NLPQL, or Bayesian optimization) to evaluate thousands of candidate designs almost instantaneously, while CFD is reserved for initial sampling and final verification[26]. Reported benefits include substantial reductions in overall optimization time, for example, approximately 72% savings using adaptive switching between CFD and an ANN surrogate, and speed-ups on the order of two magnitudes for UUV hull design using a DNN surrogate while maintaining a drag prediction error of around 1.85% MAPE[27].

In this work, Kriging (Gaussian Process Regression) is adopted as the main surrogate model because it can capture non-linear responses and provides an uncertainty-aware prediction. Other surrogate options commonly used in CFD optimisation include polynomial response surfaces, radial basis functions, and neural networks.

Polynomial Response Surface (PRS)

A second-order polynomial response surface can be written as [28]:

f ̂(x)=β_0+∑_(i=1)^kβ_i x_i+∑_(i=1)^kβ_ii x_i^2+∑_(i<j)β_ij x_i x_j+εy(x) = β0 + Σ_{i=1}^d βi xi + Σ_{i=1}^d Σ_{j=i}^d βij xi xj. (1) β (6)

β=(X^T X)^(-1) X^T yThe coefficients are estimated by least squares:

$\beta = (X^T X)^{-1} X^T y.$ (7)

Kriging (Gaussian Process Regression)

Kriging and Gaussian Process Regression (GPR) are mathematically equivalent, because both assume that the model output y(x) is a realization of a Gaussian process characterized by a mean function and a covariance structure [29]. Kriging assumes that y(x) is a realization of a Gaussian process with mean μ and covariance defined by a correlation function [30]:

f(x)μ(x)C(x,x^')f ̂(x)=μ+r^T R^(-1) (y-1μ)ŷ(x) = μ + r(x)^T R^{-1} (y − 1μ). (8)

R R is the correlation matrix between sampled designs.

r r(x) is the correlation vector between a new point and the sampled designs.

μ μ is the global mean, and 1 is a vector of ones.

The Gaussian correlation function is expressed as:

R_ij=exp⁡[ⓜ-∑_(k=1)^nθ_k |x_ikⓜ-x_jk|^(p_k)]R_ij = exp (− Σ_{k=1}^ d θ_k (x_{i,k} − x_{j,k})²). (9)

Optimization Using Surrogate Model

Once the surrogate model is trained, optimization is conducted using either metaheuristic algorithms (Genetic Algorithm, Particle Swarm Optimization) or gradient-based methods. Recent studies demonstrate the flexibility of this approach; for example, hull-form optimization for a 24,000 TEU container ship employed a random-forest surrogate combined with a modified dung-beetle optimizer to minimize total resistance [31]. Likewise, resistance minimization studies have integrated surrogate models such as RBF and Kriging with global optimizers including PSO, Differential Evolution (DE), and Artificial Bee Colony (ABC), reporting resistance reductions of up to 56% in certain cases [32].

In this work, the objective is to minimize the surrogate-predicted total resistance coefficient CR, expressed as:

"Minimize: " F(x)=f ̂(x)min C_R(x). 10)

subject to: x_L ≤ x ≤ x_U, and displacement/geometric constraints. (11)

"Subject to: " g_i (x)≤0, h_j (x)=0

Metaheuristic algorithms evaluate multiple candidates via the surrogate, reducing CFD computation cost drastically.

Validation of the surrogate model against CFD results.

Model accuracy was assessed using the coefficient of determination (R^2), root mean square error (RMSE), and mean absolute percentage error (MAPE)[33]:

R^2=1-(∑_(i=1)^N(y_i-y^_i)^2)/(∑_(i=1)^N(y_i-y ¯)^2)$R^2 = 1 - \Sigma (y_i - \hat{y}_i)^2 / \Sigma(y_i - \bar{y})^2.$ (11)

RMSE=√(1/N ∑_(i=1)^N(y_i-y^_i)^2)$RMSE = \sqrt{(1/n) \Sigma(y_i - \hat{y}_i)^2}.$ (12)

MAPE=100/N ∑_(i=1)^N 〖|(y_i-y^_i)/y_i |〗

$MAPE = (100/n) \Sigma |(y_i - \hat{y}_i)/y_i|.$ (13)

D. Optimisation Process

By integrating metaheuristic optimizers with the Kriging surrogate, the design space can be explored efficiently without running CFD for every candidate [34]. This integration substantially reduces computational cost while maintaining design feasibility constraints [35].

The optimization problem was formulated as follows:

(min⁡)┬x F(x)=C^_R (x) (14)

Subject to:

gi (x)≤0, h_j (x)=0x_i^min≤x_i≤x_i^max (15)

III. Results and Discussion

The surrogate-assisted optimisation produced an improved hull form with lower resistance than the baseline configuration while satisfying the design constraints. Figure 3 compares the CFD resistance

coefficients with the surrogate predictions and shows the corresponding residuals, indicating good agreement over the sampled design space.

Figure 3a illustrates the correlation between the CFD-computed resistance coefficients and the predicted values obtained from the Kriging surrogate model, while Figure 3b presents the residual error distribution. The data points align closely with the 45° diagonal, confirming that the surrogate reproduces the CFD response with minimal deviation. The residuals are symmetrically scattered around zero without an apparent trend, suggesting that the errors are mainly random rather than systematic. R^2=0.992.

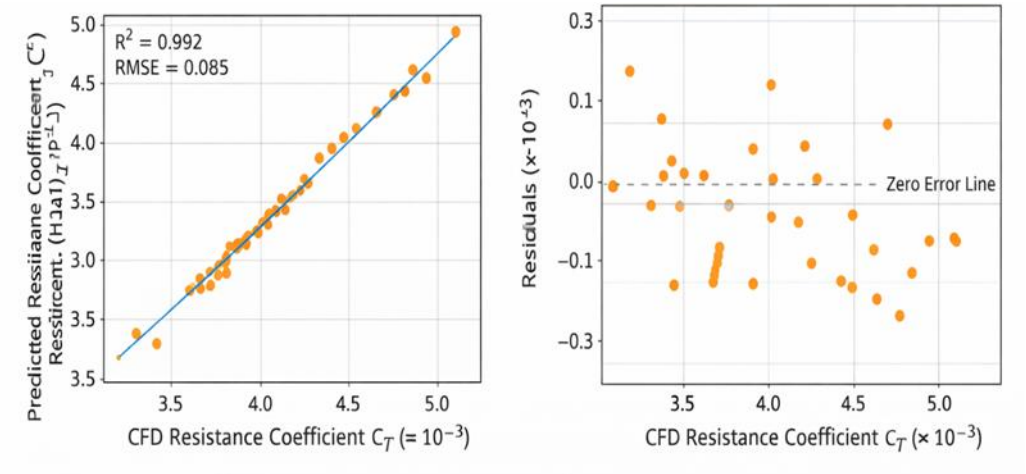

Figure 3. (a) CFD vs Surrogate Prediction; (b) Residual Error Distribution

The resistance values for the baseline and optimized hulls over Fn = 0–0.75 are summarized in Table 2. The optimized hull shows a consistent reduction across the speed range, with the maximum reduction of 14.4% occurring at Fn = 0.65.

Figure 4 compares the total resistance of the baseline and optimized hulls over Fn = 0–0.75. At low speeds (Fn < 0.3), both hulls show similar resistance because viscous drag dominates. As Fn increases, the optimized hull exhibits a slower resistance growth, indicating reduced wave-making and pressure drag in the semi-planing/planing regime.

The peak reduction of 14.4% occurs at Fn = 0.65, which is consistent with the resistance comparison in Table 2. This improvement indicates that the optimized geometry enhances longitudinal flow continuity and delays separation near the stern, resulting in better hydrodynamic efficiency for high-speed operation.

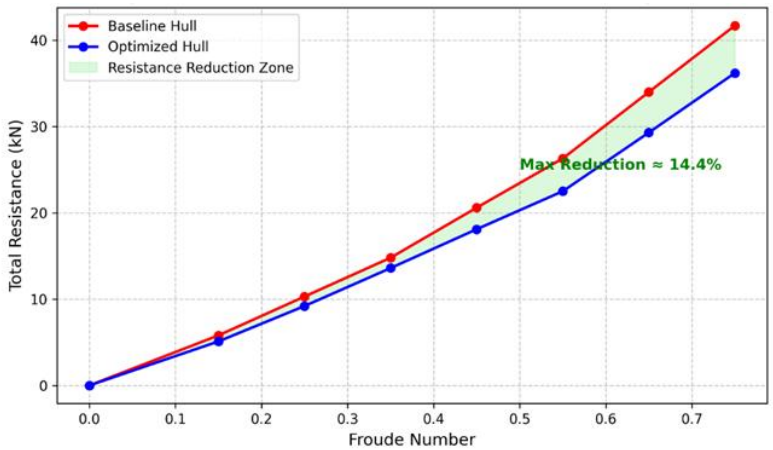

Figure 4. Total Resistance Comparison (Baseline vs Optimized)

TABLE 2.
RESISTANCE COMPARISON

Froude Number	Baseline Rt (kN)	Optimized Rt (kN)	Reduction (%)
0.00	0.0	0.0	0.0
0.15	5.8	5.1	12.1
0.25	10.3	9.2	10.7
0.35	14.8	13.6	8.1
0.45	20.6	18.1	12.2
0.55	26.3	22.5	14.4
0.65	34.0	29.3	13.7
0.75	41.7	36.2	13.2

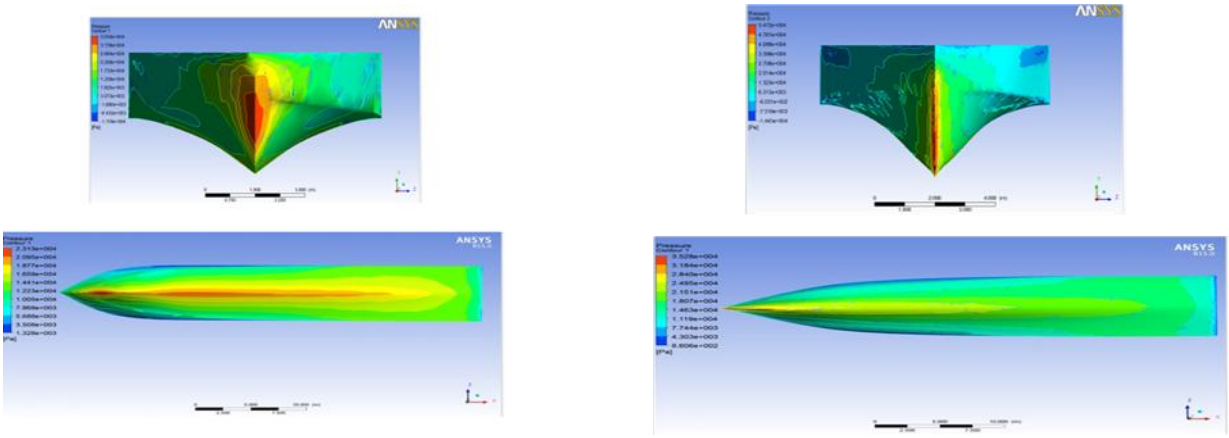

Figure 5. Pressure Distribution on the Hull Surface (baseline vs optimized)

Figures 5 and 6 present CFD post-processing results for the baseline and optimized hull configurations. In Figure 5 (pressure contours), the baseline hull shows a pronounced high-pressure region near the bow due to flow stagnation and a larger low-pressure region toward the stern, indicating earlier separation. In contrast, the optimized hull exhibits a smoother pressure gradient along the bottom and improved pressure recovery near the transom. The streamline patterns in Figure 6 further indicate reduced wake vortices and more uniform flow behind the hull, which is consistent with the observed resistance reduction.

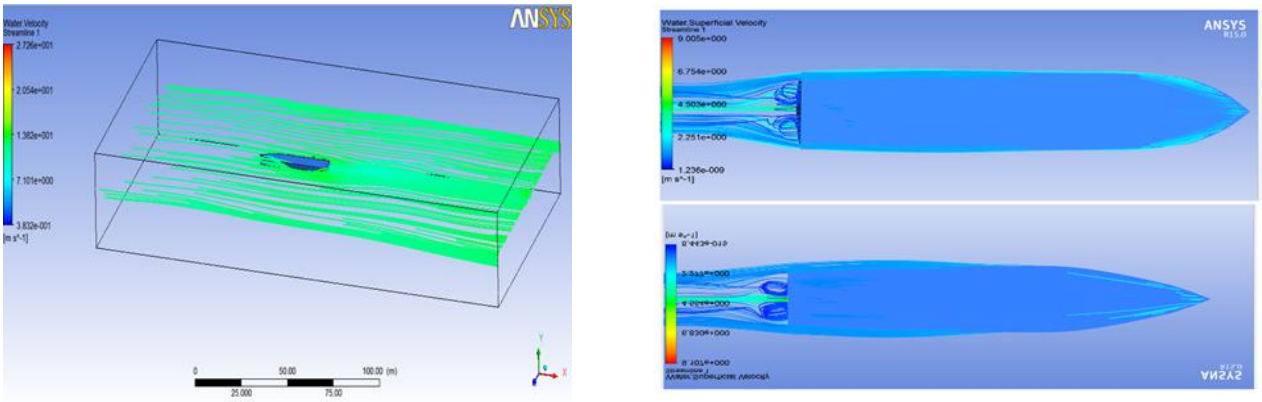

Figure 6. Velocity Streamlines for Baseline and Optimized Hulls

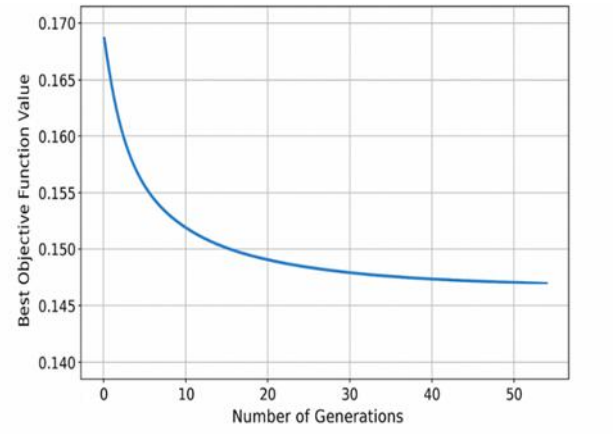

Figure 7. Convergence curve of the Genetic Algorithm (GA)

Overall, the CFD contours confirm that the surrogate-assisted optimisation leads to improved flow characteristics: reduced bow pressure peaks, smaller separated regions near the stern, and a more uniform pressure distribution over the wetted surface. These physical observations support the quantitative resistance reductions reported in Table 2 and Figure 4.

Figure 7 depicts the convergence curve of the Genetic Algorithm (GA) used in the surrogate-assisted optimization. The objective value decreases rapidly in the early generations as the algorithm explores the design space and then gradually stabilizes as it converges toward an optimum. The smooth trend indicates that the Kriging surrogate provides a stable response surface for the GA search.

IV. Conclusion

This study developed a surrogate-assisted optimisation framework that integrates RANS CFD, Kriging (GPR) modelling, and metaheuristic search (GA and PSO) to reduce the resistance of a fast-boat hull. The Kriging surrogate achieved high predictive accuracy (R^2 = 0.985, prediction error < 2%) while reducing the required CFD effort by about 78% compared with a CFD-only search. CFD verification shows that the optimized hull provides a consistent resistance reduction over Fn = 0–0.75, with a maximum reduction of 14.4% at Fn = 0.65. Flow visualisations confirm reduced bow pressure peaks and delayed stern separation. The proposed workflow is suitable for efficient early-stage hull-form design and can be extended to include multi-objective criteria such as stability and seakeeping.

Acknowledgements

The authors would like to express their sincere gratitude to Politeknik Negeri Bengkalis for the research facilities and academic support provided during this study. Special thanks are also extended to the Pusat Penelitian dan Pengabdian kepada Masyarakat (P3M) Politeknik Negeri Bengkalis for funding assistance and continuous encouragement in the development of applied maritime research. Their contribution and commitment have been instrumental in the successful completion of this work

References

[1] L. Cui, Z. Chen, and Y. Feng, “Numerical study on the mechanism of drag reduction for interceptors on planing boats,” Modern Physics Letters B, vol. 35, no. 32, Nov. 2021, doi: 10.1142/S0217984921400236.

[2] R. Tayeb, S. E. Belhenniche, M. Belkadi, M. A. Rizk, O. K. Kinaci, and P. Liu, “Optimizing Geometric Parameters of Planing Vessels for Enhanced Hydrodynamic Performance,” Journal of Marine Science and Application, vol. 24, no. 5, pp. 970–983, Oct. 2025, doi: 10.1007/s11804-025-00632-5.

[3] M. Sulman, S. Mancini, and R. N. Bilandi, “Numerical Investigation of Single and Double Steps in Planing Hulls,” J Mar Sci Eng, vol. 12, no. 4, p. 614, Apr. 2024, doi: 10.3390/jmse12040614.

[4] R. Niazmand Bilandi, A. Dashtimanesh, S. Mancini, and L. Vitiello, “Comparative study of experimental and CFD results for stepped planing hulls,” Ocean Engineering, vol. 280, p. 114887, Jul. 2023, doi: 10.1016/j.oceaneng.2023.114887.

[5] A. Moghaddas and H. Zeraatgar, “Investigation of the static trim angle effects on the hydrodynamic performances of a semi-planing catamaran in calm water and waves,” Scientia Iranica, vol. 0, no. 0, pp. 0–0, Sep. 2024, doi: 10.24200/sci.2024.61884.7544.

[6] S. Samuel, O. Mursid, S. Yulianti, Kiryanto, and M. Iqbal, “EVALUATION OF INTERCEPTOR DESIGN TO REDUCE DRAG ON PLANING HULL,” Brodogradnja, vol. 73, no. 3, pp. 93–110, Sep. 2022, doi: 10.21278/brod73306.

[7] A. Coppedè, S. Gaggero, G. Vernengo, and D. Villa, “Hydrodynamic shape optimization by high fidelity CFD solver and Gaussian process based response surface method,” Applied Ocean Research, vol. 90, p. 101841, Sep. 2019, doi: 10.1016/j.apor.2019.05.026.

[8] P. Wang, Y. Feng, Z. Chen, and Y. Dai, “Study of a hull form optimization system based on a Gaussian process regression algorithm and an adaptive sampling strategy, Part I: Single-objective optimization,” Ocean Engineering, vol. 279, p. 114502, Jul. 2023, doi: 10.1016/j.oceaneng.2023.114502.

[9] P. Renaud, M. Sacher, and Y.-M. Scolan, “Multi-objective hull form optimization of a SWATH configuration using surrogate models,” Ocean Engineering, vol. 256, p. 111209, Jul. 2022, doi: 10.1016/j.oceaneng.2022.111209.

[10] X. Liu, W. Zhao, and D. Wan, “Multi-fidelity Co-Kriging surrogate model for ship hull form optimization,” Ocean Engineering, vol. 243, p. 110239, Jan. 2022, doi: 10.1016/j.oceaneng.2021.110239.

[11] H. Pehlivan Solak, “MULTI-DIMENSIONAL SURROGATE BASED AFT FORM OPTIMIZATION OF SHIPS USING HIGH FIDELITY SOLVERS,” Brodogradnja, vol. 71, no. 1, pp. 85–100, Mar. 2020, doi: 10.21278/brod71106.

[12] S. G. Kontogiannis and M. A. Savill, “A generalized methodology for multidisciplinary design optimization using surrogate modelling and multifidelity analysis,” Optimization and Engineering, vol. 21, no. 3, pp. 723–759, Sep. 2020, doi: 10.1007/s11081-020-09504-z.

[13] X. Liu, W. Zhao, and D. Wan, “Multi-fidelity Co-Kriging surrogate model for ship hull form optimization,” Ocean Engineering, vol. 243, p. 110239, Jan. 2022, doi: 10.1016/j.oceaneng.2021.110239.

[14] P. Wang, Y. Feng, Z. Chen, and Y. Dai, “Study of a hull form optimization system based on a Gaussian process regression algorithm and an adaptive sampling strategy, Part I: Single-objective optimization,” Ocean Engineering, vol. 279, p. 114502, Jul. 2023, doi: 10.1016/j.oceaneng.2023.114502.

[15] F. A. Rayhan, A. Masrul, A. Khairullah Akbar, and B. Anugerah Putra, “Numerical Study on Resistance of Stepped Planing Hull,” Journal of Mechanical Engineering Science and Technology (JMEST), vol. 7, no. 2, p. 106, Sep. 2023, doi: 10.17977/um016v7i22023p106.

[16] A. Windyandari, S. Sugeng, M. Ridwan, and A. K. Yusim, “Study on resistance performance of hexagonal hull form with variation of angle of attack, deadrise, and stern for flat-sided catamaran vessel,” Curved and Layered Structures, vol. 11, no. 1, Nov. 2024, doi: 10.1515/cls-2024-0016.

[17] J. Chen, Y. Ou, G. Xiang, Q. Ye, and W. Wang, “A Parametric Design Method for Unstepped Planing Hulls Using Longitudinal Functions and Shape Coefficients,” Applied Sciences, vol. 15, no. 5, p. 2667, Mar. 2025, doi: 10.3390/app15052667.

[18] T. N. Tu, T.-H. Le, D. M. Thien, T. Van Tao, and V. M. Ngoc, “Numerical Study of the Effect of River-Sea Ship Hull Form Parameters on Resistance and Their Optimisation Using the Taguchi-Grey Method,” Polish Maritime Research, vol. 32, no. 2, pp. 17–28, Jun. 2025, doi: 10.2478/pomr-2025-0017.

[19] A. Sulisetyono and M. Alifrananda, “Evaluation of the ship resistance using computational fluid dynamics at various Froude numbers,” in Proceedings of the 1st International Conference on Sustainable Engineering Development and Technological Innovation, ICSEDTI 2022, 11-13 October 2022, Tanjungpinang, Indonesia, EAI, 2023. doi: 10.4108/eai.11-10-2022.2326428.

[20] R. Akbar, I. K. Suastika, and I. K. A. P. Utama, “Effects of Homogeneous and Inhomogeneous Roughness on the Ship Resistance,” CFD Letters, vol. 17, no. 3, pp. 77–94, Oct. 2024, doi: 10.37934/cfdl.17.3.7794.

[21] K. Song et al., “Simulation strategy of the full-scale ship resistance and propulsion performance,” Engineering Applications of Computational Fluid Mechanics, vol. 15, no. 1, pp. 1321–1342, Jan. 2021, doi: 10.1080/19942060.2021.1974091.

[22] A. Firdhaus, Kiryanto, A. F. Zakki, M. L. Hakim, and H. Khalis, “Impact of Surface Roughness on Interference Resistance in Delft 372 Catamarans,” International Journal of Automotive and Mechanical Engineering, vol. 22, no. 3, pp. 12547–12559, Sep. 2025, doi: 10.15282/ijame.22.3.2025.1.0958.

[23] Y. Kong, S. Zhang, J. Zhang, and Y. Zheng, “Inflow and outflow numerical simulation using least-square moving particle semi-implicit method on GPU,” Comput Part Mech, vol. 11, no. 2, pp. 627–641, Apr. 2024, doi: 10.1007/s40571-023-00643-5.

[24] L. Du, Q. Wu, Y. Shu, and G. Li, “The effects of online-training artificial neural network mechanism and multi-stage parametric modeling method on simulation-based design system for ship optimization,” Ocean Engineering, vol. 309, p. 118284, Oct. 2024, doi: 10.1016/j.oceaneng.2024.118284.

[25] Y. Shen et al., “Application of Machine Learning for Bulbous Bow Optimization Design and Ship Resistance Prediction,” Applied Sciences, vol. 15, no. 6, p. 2934, Mar. 2025, doi: 10.3390/app15062934.

[26] L. Zheng, S. Yan, X. Chen, B. Kun, and S. Chen, “Multi-Surrogate Model Aided Bow Optimization of River and Coastal Connection Ship,” in Volume 5B: Ocean Engineering, American

Society of Mechanical Engineers, Jun. 2024. doi: 10.1115/OMAE2024-126645.

[27] H. Vardhan, D. Hyde, U. Timalsina, P. Volgyesi, and J. Sztipanovits, "Sample-efficient and surrogate-based design optimization of underwater vehicle hulls," Ocean Engineering, vol. 311, p. 118777, Nov. 2024, doi: 10.1016/j.oceaneng.2024.118777.

[28] X.-G. Wang, M. M. A., B. Zhao, W.-H. Zhang, and S. Song, "Response Surface Model Optimization Algorithm for Structural Assessment Based on Vibration Frequency," Shock and Vibration, vol. 2025, no. 1, Jan. 2025, doi: 10.1155/vib/5446251.

[29] J. Ching and I. Yoshida, "Efficient simulation of 3D conditional random field using kriging with Gaussian-process trend," Comput Geotech, vol. 177, p. 106862, Jan. 2025, doi: 10.1016/j.compgeo.2024.106862.

[30] A. Marrel and B. Iooss, "Probabilistic surrogate modeling by Gaussian process: A review on recent insights in estimation and validation," Reliab Eng Syst Saf, vol. 247, p. 110094, Jul. 2024, doi: 10.1016/j.ress.2024.110094.

[31] H. Zhang, Y. Wei, S. Xiao, and Z. Zhao, "Ship hull resistance minimization using surrogate modelling and an improved dung beetle optimizer," Ocean Engineering, vol. 322, p. 120588, Apr. 2025, doi: 10.1016/j.oceaneng.2025.120588.

[32] J. Feng, S. Ye, Y. Zhang, L. Qi, and Y. Shen, "A comparative study of combined surrogate models and evolutionary algorithms for ship resistance optimization," in Fourth International Conference on Mechanical, Electronics, and Electrical and Automation Control (METMS 2024), J. Zhang, Z. H. Khan, and P. Zeng, Eds., SPIE, Jun. 2024, p. 101. doi: 10.1117/12.3030217.

[33] H. M. Tran, T. M. Le, K. Wang, H. V. Pham, K. Y. Ngo, and S. V. T. Dao, "Precise 2D vision solutions for estimating avocado physical characteristics," Sci Rep, vol. 15, no. 1, p. 35377, Oct. 2025, doi: 10.1038/s41598-025-19238-6.

[34] Y. Guo, Y. Wang, Y. Cao, and Z. Long, "A New Optimization Design Method of Multi-Objective Indoor Air Supply Using Kriging Model and NSGA-II," Aug. 21, 2023. doi: 10.20944/preprints202308.1376.v1.

[35] N. Pholdee, S. Bureerat, W. Nuantong, and B. Pongsatitpat, "Kriging Surrogate-based Optimization for Shape Design of Thin Electric Propeller," Journal of Engineering and Technological Sciences, vol. 56, no. 3, pp. 404–413, Jun. 2024, doi: 10.5614/j.eng.technol.sci.2024.56.3.8.